This is an *Accepted Manuscript*, which has been through the RSC Publishing peer review process and has been accepted for publication.

Accepted Manuscripts are published online shortly after acceptance, which is prior to technical editing, formatting and proof reading. This free service from RSC Publishing allows authors to make their results available to the community, in citable form, before publication of the edited article. This *Accepted Manuscript* will be replaced by the edited and formatted *Advance Article* as soon as this is available.

To cite this manuscript please use its permanent Digital Object Identifier (DOI®), which is identical for all formats of publication.

More information about *Accepted Manuscripts* can be found in the **Information for Authors**.

Please note that technical editing may introduce minor changes to the text and/or graphics contained in the manuscript submitted by the author(s) which may alter content, and that the standard **Terms & Conditions** and the **ethical guidelines** that apply to the journal are still applicable. In no event shall the RSC be held responsible for any errors or omissions in these *Accepted Manuscript* manuscripts or any consequences arising from the use of any information contained in them.

Dynamic Article Links ▶

COMMUNICATION

A one-pot solvothermal strategy for hierarchical microspheres with radially assembled single-crystalline TiO₂-nanorods as high performance photoanode materials in dye-sensitized solar cells†

Ziming He, Jing Liu, Jianwei Miao, Bin Liu, and Timothy Thatt Yang Tan*

A simple, one-pot method to prepare complex morphology-tunable hierarchical TiO₂ microspheres consisting of radially assembled single-crystal rutile TiO₂ nanorods is developed by
10 **combining an acid thermal crystallization and a self-assembly process of the nanorods via a solvothermal amphiphile-water microreactor strategy. Using P25 nanoparticles as a void filler to generate a mesoporous electrode film, the microsphere based photoanode exhibits a maximum power conversion**
15 **efficiency of 7.95% at an anode film thickness of 27.2 μm, highlighting the importance of material architecture tailoring in improving the electron transport properties of dye-sensitized solar cells.**

Dye-sensitized solar cells (DSSCs) have been extensively
20 investigated as one of the most promising low-cost alternatives to conventional silicon based photovoltaics.[1] The main components of DSSCs are a Pt cathode, a redox-active electrolyte and a photoanode consisting of a dye-sensitized semiconductor nanocrystalline film deposited on a transparent conducting
25 substrate. A high-performance photoanode is expected to possess large specific surface area for sufficient dye loading, strong scattering effect to compensate the low light absorption efficiency of the sensitizer (typically N719 or N3) in the red region, and effective electron transport to reduce charge recombination.
30 However, the above features usually negate each other for nanocrystalline based anode films.[2] For instance, thick photoanode films prepared using TiO₂ nanoparticles exhibit large specific surface area, inevitably accompanied by a large amount of grain boundaries, which is unfavourable for efficient electron
35 transport in the TiO₂ matrix. Besides, strong scattering effect requires large particles, the specific surface area of which is usually low, leading to reduction of dye loading.

Recently, hierarchical TiO₂ microspheres have been synthesized and investigated as the photoanode materials.[3, 4] The
40 microspheres are capable of enhancing the scattering effect of the photoanode due to its micron size while maintaining or even increasing the surface area due to its nanoscale primary unit, such as nanoparticles and nanosheets, thus improving the DSSC performance. Single-crystal rutile TiO₂ nanorod exhibits fast
45 electron transport rate due to its high electron diffusion coefficient arising from their low density of sub-bandgap defect states.[5, 6] To integrate the effects of large specific surface area,
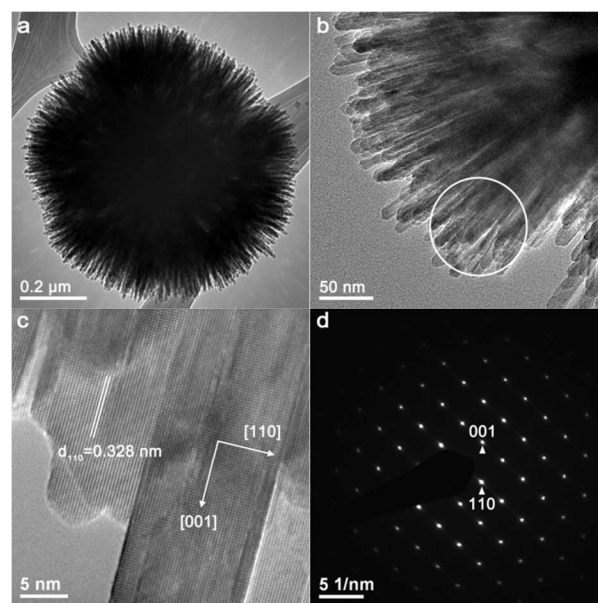

Fig. 1 (a, b) TEM and (c) HRTEM images of T150, and (d)
50 corresponding SAED pattern to white circled part of (b).

strong scattering and efficient electron transport into a single photoanode, hierarchical microspheres constructed with single crystal rutile TiO₂ nanorods have been developed and utilized to prepare the DSSC anodes through direct growth[7] and screen
55 printing[8] of the microspheres on transparent conducting substrate. However, the former approach may face challenges in production scale up and film thickness control. For the latter, Na⁺ residues derived from sodium salts involved in the microsphere synthesis process can limit the power conversion efficiency (PCE) of
60 DSSCs,[9] therefore demonstrating a modest 3.57% in PCE, only 13% enhancement compared to P25 based anodes at a film thickness of 16 μm. Besides, big rod bundles with a diameter of more than 100 nm formed by densely packed nanorods in microspheres decrease the surface area of the photoanodes, only
65 giving a PCE of 2.94% at an anode film thickness of ~20 μm.[10]

Herein, we demonstrate a facile solvothermal strategy to prepare single-crystal rutile TiO₂ nanorods constructed microspheres. The nanorods are radially assembled without the formation of rod bundles and their diameters are carefully
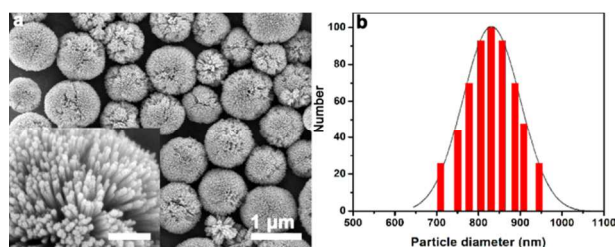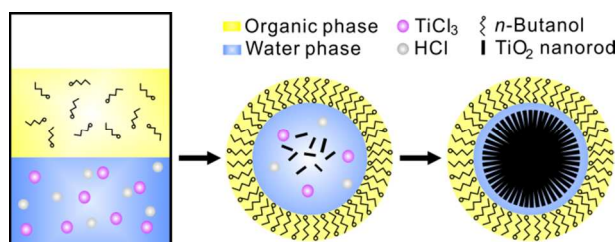70 controlled for high specific surface area. The conceived strategy

Fig. 2 (a) SEM image and (b) particle size distribution diagram of T150. Inset of (a) is a magnification image and the scale bar is 200 nm.

Scheme 1 The procedure of the facile solvothermal approach.

involves the use of *n*-butanol as an amphiphile for the formation of microreactors in which an acid thermal crystallization process and a self-assembly process of the TiO_2 nanorods into microspheres occur during the one-step solvothermal reaction. Instead of titanium alkoxides, $TiCl_3$ is utilized as the Ti source, which has the attractive attributes of high water solubility to enable rutile TiO_2 nanorods formation in the water-rich microreactors, as well as high stability and low cost.[11] In addition, the current method does not require any pre-treatment, such as the mixing of the reaction precursor by stirring or sonication, thus making this approach very simple for particle morphology tunability and economical for large scale production. Briefly, $TiCl_3$ acidic aqueous solution diluted with equivoluminal DI water were added into a Teflon-lined autoclave, followed by the addition of *n*-butanol. Subsequently, the autoclave was sealed and placed in an oven at 150°C for 4h. After natural cooling to room temperature, the product was washed using centrifuge and dried in air (please find experiment details in ESI†). The obtained powder, labelled as T150, was used as the photoanode material and the device performance was systematically evaluated.

TEM images of the as-prepared T150 in Fig. 1a and 1b exhibit a dandelion-like spherical morphology, consisting of numerous TiO_2 nanorods radiating from the center with an average diameter of 14 nm. From HRTEM image, the lattice distance highlighted in Fig. 1c was determined to be 0.328 nm, which corresponds to rutile (110) planes, indicating that the nanorod growth direction is along the [001] orientation.[12] The selected area electron diffraction (SAED) pattern in Fig. 1d confirms the single-crystalline nature of the TiO_2 nanorods, which is very crucial for DSSC, as fast electron transport through the single-crystal nanorods can be achieved with minimal charge recombination. Besides, the smooth side surfaces and high crystallinity of the nanorods are capable of suppressing the electron trapping at surface defects.[7] Fig. 2a shows the FESEM image of T150 microspheres with radially assembled nanorods but without the formation of rod bundles, which brings about a high specific surface area. The size distribution of the microspheres was also examined and the result is displayed in Fig. 2b, showing that the mean diameter of T150 microspheres is 831 nm.
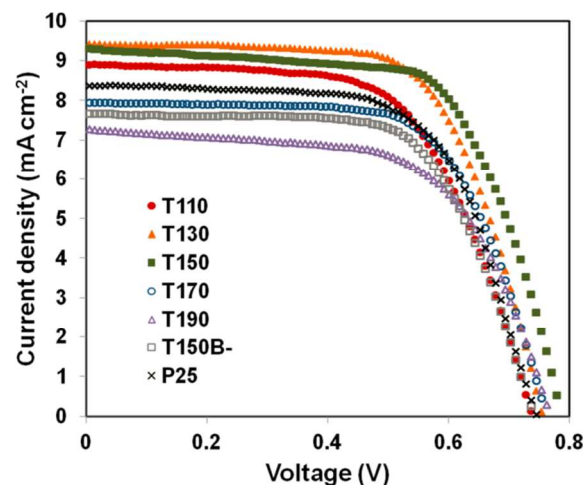

Fig. 3 *J*-V characteristics of the seven devices with different anodes.

TEM image in Fig. S1a exhibits a rod-like morphology of a control sample synthesized in the same condition as the T150 but without the addition of *n*-butanol. The diameter of the TiO_2 nanorods is ~14 nm and the rod length varies in the range of 14-80 nm. Based on the comparison of the morphology of T150 and its control sample (labelled as T150B-), a formation mechanism of the hierarchical microspheres is proposed and presented in Scheme 1. The water-rich microreactor droplets formed by an amphiphile-water system is an ideal soft template for self-assembly of the nanocrystals into a three dimensional microstructure.[12] Highly acid condition and selective adsorption of Cl^- on rutile (110) plane favours the formation of rutile phase and promotes the anisotropic growth of TiO_2 into nanorods along [001] orientation.[13] Therefore, random TiO_2 nanorods form in the water phase in the presence of HCl (from the acidic $TiCl_3$ solution) at the beginning of the reaction. Cl^- adsorption on the (110) plane gives rise to repulsive forces between the side walls of the nanorods.[14] Consequently, the nanorods joint on the (001) plane (the highest energy plane of rutile TiO_2) and assemble into spherical structure in the microreactors to minimize their surface area and reduce the total free energy.[15] The repulsive force between the nanorods avoids the aggregation of the nanorods into rod bundles, hence ensuing a more loosely-packed structure and a larger specific surface area of the microspheres, laying the foundation for high performance DSSC. The grooves at the edges and joints of the assembled nanorods are favourable sites for adatom attachment to form new atomic layers and eventually new single crystals with smooth side surface.[16] As the reaction progresses, microspheres increase in size, finally forming hierarchical TiO_2 microspheres consisting of radially assembled single-crystal rutile TiO_2 nanorods. On the contrary, without the restriction of the microreactors, the random TiO_2 nanorods can move freely in Brownian motion within the reaction precursor and thus are unable to assemble into the microspheres.

To investigate the effect of reaction temperature, solvothermal syntheses were carried out at 110, 130, 170 and 190 °C to prepare a series of samples, which were labelled with the corresponding reaction temperature. We observed a temperature-dependent morphological evolution of the microspheres (evident in Fig. S2 and Table S1). As the reaction temperature increases, the particle size of the microspheres decreases while the diameter of nanorod
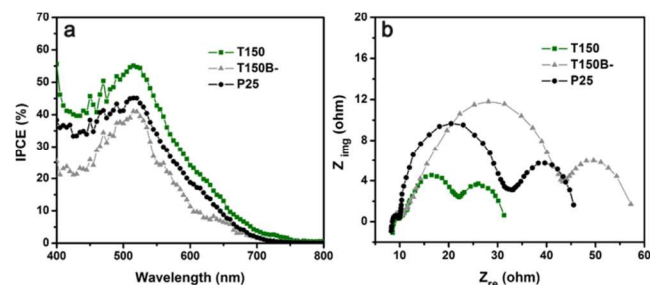
Fig. 4 (a) IPCE and (b) Nyquist plots of the devices based on T150, T150B- and P25.

Table 1 Photovoltaic performance of the T150:P25 (60:40 wt ratio) composite devices

Thickness (μm)	J_{sc} (mA cm^{-2})	V_{oc} (V)	FF (%)	PCE (%)
9.1	10.4	0.830	65.7	5.69
13.7	13.8	0.788	58.4	6.35
18.2	15.4	0.779	57.7	6.93
22.6	17.1	0.762	57.2	7.46
27.2	18.8	0.745	56.7	7.95
29.3	18.1	0.736	56.5	7.52

increases, which can be attributed to enhanced mixing of water and *n*-butanol to generate a smaller water phase "microreactor" and a faster growth kinetic of nanorod induced by high temperature. Moreover, the spacing of the nanorods was observed to become larger with increasing temperature, and destruction of the spheres occurred at 190 °C, indicating the loss in stability of the microemulsion at this temperature. The specific surface area of the microspheres is inevitably affected by the above morphological changes and determined to be 84.69, 97.07, 89.24, and 63.68 m^2 g^{-1} for T110, T130, T150 and T170, respectively. The surface area of T190 is 49.28 m^2 g^{-1}, lower than that (58.18 m^2 g^{-1}) of P25, while the T150B- shows the highest surface area of 97.54 m^2 g^{-1}. XRD patterns of T110, T130, T150 and T150B- primarily exhibit characteristic peaks of rutile TiO$_2$ as shown in Fig. S3, which is consistent with HRTEM observation. For T170 and T190, the peaks corresponding to anatase TiO$_2$ appear. We speculate that at higher temperatures, there may be less HCl for the anisotropic growth of rutile nanorods due to the increased dissolution of HCl in *n*-butanol. The crystallinity of the microspheres is improved at high reaction temperature, which is revealed by the decreased full-width-half-maxima of the diffraction peaks. UV-Vis DRS in Fig. S4 show that the reflectance of the microspheres is more than 80% in the range of 450-800 nm, which is higher than that (around 70%) of P25 and T150B-, confirming the enhanced light-scattering property of the microspheres.

The five hierarchical TiO$_2$ microspheres, as well as the P25 and T150B- (as reference), were utilized to prepare photoanodes using a doctor-blade technique. The active area and film thickness of the anodes were controlled to be 0.2 cm^2 and 9 μm, respectively. Fig. 3 shows the photocurrent density-voltage (*J*-V) characteristics of the seven devices, the performance parameters of which are summarized in Table S2 for comparison. For the hierarchical microspheres, the trend of short-circuit current density (*J*$_{sc}$) of the photoanodes corresponds to their specific surface areas, indicating that the *J*$_{sc}$ is mainly determined by the dye loading. With the highest specific surface area, T130 based device gives the highest *J*$_{sc}$ of 9.48 mA cm^{-2}, while the *J*$_{sc}$ of the device based on T110, T150, T170 and T190 is 8.89, 9.32, 7.91 and 7.36 mA cm^{-2}, respectively. P25 based photoanode delivers a *J*$_{sc}$ of 8.31 mA cm^{-2}, higher than that of T170 based photoanode and close to that of T150 based device. Anatase TiO$_2$ nanoparticle-based anodes usually exhibit high surface area per unit film volume and consist of high surface -OH group density, which enhances dye loading.[17] These reasons may contribute to the high *J*$_{sc}$ of P25 based device. Rutile nanocrystals, in general,

show superior light-scattering characteristics and single-crystal rutile TiO$_2$ nanorods, with a length up to several hundreds of nanometers, are capable of enhancing the charge collection efficiency of DSSC photoanodes.[18] Although T150B- exhibits the highest specific surface area, its photoanode only delivers a *J*$_{sc}$ of 7.66 mA cm^{-2}. The lower current density may be resultant from the relatively lower scattering effect and electron transport rate through the randomly arranged TiO$_2$ nanorods with smaller diameter and length, reinforcing the importance of the hierarchical structure of the microspheres in photoanode performance enhancement. Open-circuit voltage (*V*$_{oc}$) and fill factor (FF) of the microspheres based devices are generally higher than those of P25 and T150B- reference cells, which indicates efficient electron transfer in the photoanodes consisting of hierarchical microspheres of single-crystal rutile TiO$_2$ nanorods with few-hundreds nanometer length. *V*$_{oc}$ and FF increase from T110 to T150 based photoanodes, which reflects the reduced internal resistance probably resulted from the enhanced electron transport in TiO$_2$ nanorods with improved crystallinity at higher temperature. Compared to T150, the *V*$_{oc}$ and FF of T170 and T190 based devices decrease, which is ascribed to the formation of the anatase phase in these two samples, which will probably reduce electron transport efficiency compared to single-crystal rutile TiO$_2$ nanorods. With a large surface area (89.24 m^2 g^{-1}), enhanced scattering effect (~18% reflectance improvement compared to P25), and efficient electron transport (highly crystalline rutile TiO$_2$ single-crystal nanorods), T150 based device delivers the highest PCE of 4.90%, more than 20% higher than conventional P25 reference cell (4.06%).

Incident photon-to-current conversion efficiency (IPCE) and electrochemical impedance spectra (EIS) of T150, T150B- and P25 based devices were measured to offer a physical insight into the effect of the TiO$_2$ microspheres on DSSC performance enhancement. Fig. 4a displays the IPCE curves as a function of wavelength. The enhanced IPCE of T150 based device over a wide range of 400-750 nm is attributed to the increased light harvesting efficiency from improved dye loading, light reflectance and electron transport.[4] Nyquist plots of the devices in Fig. 4b illustrate three semicircles, the diameters of which represent the impedance of the corresponding processes. The first semicircles measured in the high-frequency (kHz) range represent the Faraday resistance of the redox reaction of I$^-$/I^{3-} at the Pt/electrolyte interface. The second semicircles in medium-frequency (1-100 Hz) range reflect the electron transfer resistance at the TiO$_2$/dye/electrolyte interface, which is the most decisive factor in DSSCs. The third semicircles obtained in low-frequency (mHz) range are related to the Warburg diffusion process of I^{3-} in the electrolyte.[19] As the counter electrodes are exactly the same for all devices, the Faraday resistance of the three cells exhibit

similar diameter values. Compared to the second semicircle diameter of P25 (~22.3 ohm) and T150B- (~35.9 ohm) reference cells, an obvious decrease in that of the T150 device (~14.7 ohm) is observed, which indicates enhanced charge transport of the T150 based photoanodes, attributed to the fast electron transport in the long (> 800 nm) single-crystal rutile TiO_2 nanorods with less grain boundaries and lower density of sub-bandgap defect states.[5, 17] The inefficient electron transport in T150B- anode is confirmed by the large diameter of its second semicircle. The high impedance may be associated with the large number of grain boundaries between the small-sized nanorods with disfavours electron transport.[20] The third semicircle of the T150 based device exhibits a slightly smaller diameter compared to that of P25 and T150B- reference cells, which could be attributed to the bigger inter-particles pores that facilitate the diffusion of I^{3-} in the photoanode.[2]

From the SEM images of the anode films (Fig. S5), numerous voids can be observed in the T150 based photoanode. The presence of these large voids generates dead space and reduce dye adsorption. We therefore undertook a strategy to use P25 as a void filler, due to its smaller size and ~80% of anatase phase which could improve dye loading of the T150 based photoanode. The weight ratio of T150 and P25 was adjusted to 60:40 to achieve a mesoporous electrode film of high void filling (Fig. S5d). The devices prepared using this ratio were optimized by adjusting the anode film thickness and the photovoltaic performances of all the devices are summarized in Table 1. The J_{sc} increases while the V_{oc} and FF decrease with increasing film thickness. The composite photoanode with the thickness of 9.1 μm gives a PCE of 5.69%, ~16% and 40% higher than T150 and P25 based solar cells with the same thickness. The optimal PCE (7.95%) is obtained at an anode film thickness of 27.2 μm, with the J_{sc} of 18.8 mA cm^{-2}, V_{oc} of 0.745 and FF of 56.7%. The optimal film thickness of the nanoparticle based photoanodes is generally 10-14 μm corresponding to the typical electron diffusion length of such films.[21] The increased optimal film thickness of the current T150 based composite anode reflects the improved electron diffusion in the anode film due to the incorporation of the hierarchical TiO_2 microspheres. Therefore, this study has shown that the electron transport property of DSSC photoanode film can be enhanced through careful materials architecture tailoring and design.

Conclusions

We have developed a simple synthetic method to prepare complex hierarchical TiO_2 microspheres constructed with radially assembled single-crystal rutile TiO_2 nanorods by combining an acid thermal crystallization and a self-assembly process of the nanorods via a solvothermal amphiphile-water microreactor strategy. The morphology and crystallinity of the hierarchical microspheres are temperature dependent, which allows the control of the diameter and spacing of the nanorods by adjusting the reaction temperature to endow the microspheres with high specific surface area as superior photoanode materials. A significant improvement (20%) in PCE for T150 based device is achieved compared to the conventional P25 reference cell, which is contributed to the synergistic effects of the large specific surface area, enhanced scattering effect, and efficient electron transport property of the T150 microspheres. Using P25 nanoparticles as a void filler, the T150 based photoanode exhibits a maximum PCE of 7.95% at an anode film thickness of 27.2 μm. The current one-pot solvothermal synthetic strategy may be extended for the preparation of other types of metal oxide microspheres with nano-micro hierarchical structure.

Notes and references

School of Chemical and Biomedical Engineering, Nanyang Technological University, 62 Nanyang Drive, Singapore 637459.
E-mail: tytan@ntu.edu.sg; Fax: +65-67911761

† Electronic Supplementary Information (ESI) available: Detailed experimental procedures, TEM images, SEM images, XRD patterns, DRS spectra, size distribution data, BET data, and performance parameters of all samples. See DOI: 10.1039/b000000x/

1. M. Gratzel, *Nature*, 2001, **414**, 338; L. L. Li and E. W. G. Diau, *Chem. Soc. Rev.*, 2013, **42**, 291; A. Yella, H. W. Lee, H. N. Tsao, C. Y. Yi, A. K. Chandiran, M. K. Nazeeruddin, E. W. G. Diau, C. Y. Yeh, S. M. Zakeeruddin and M. Gratzel, *Science*, 2011, **334**, 629.
2. F. Zhu, D. P. Wu, Q. Li, H. Dong, J. M. Li, K. Jiang and D. S. Xu, *RSC Adv.*, 2012, **2**, 11629.
3. K. Fan, T. Y. Peng, J. N. Chen, X. H. Zhang and R. J. Li, *J. Power Sources*, 2013, **222**, 38; W. Q. Fang, X. H. Yang, H. J. Zhu, Z. Li, H. J. Zhao, X. D. Yao and H. G. Yang, *J. Mater. Chem.*, 2012, **22**, 22082; J. Y. Liao, H. P. Lin, H. Y. Chen, D. B. Kuang and C. Y. Su, *J. Mater. Chem.*, 2012, **22**, 1627; D. P. Wu, F. Zhu, J. M. Li, H. Dong, Q. Li, K. Jiang and D. S. Xu, *J. Mater. Chem.*, 2012, **22**, 11665; W. G. Yang, J. M. Li, Y. L. Wang, F. Zhu, W. M. Shi, F. R. Wan and D. S. Xu, *Chem. Commun.*, 2011, **47**, 1809.
4. J. Y. Liao, B. X. Lei, D. B. Kuang and C. Y. Su, *Energy Environ. Sci.*, 2011, **4**, 4079.
5. X. J. Feng, K. Zhu, A. J. Frank, C. A. Grimes and T. E. Mallouk, *Angew. Chem. Int. Ed.*, 2012, **51**, 2727.
6. B. Liu and E. S. Aydil, *J. Am. Chem. Soc.*, 2009, **131**, 3985.
7. Z. Q. Sun, J. H. Kim, Y. Zhao, D. Attard and S. X. Dou, *Chem. Commun.*, 2013, **49**, 966.
8. J. Sheng, L. H. Hu, W. X. Li, L. E. Mo, H. J. Tian and S. Y. Dai, *Solar Energy*, 2011, **85**, 2697.
9. X. Wu, G. Q. Lu and L. Z. Wang, *J. Colloid Interface Sci.*, 2013, **391**, 70.
10. M. D. Ye, H. Y. Liu, C. J. Lin and Z. Q. Lin, *Small*, 2013, **9**, 312.
11. B. Xue, T. Sun, F. Mao, L. C. Sun, W. Yang, Z. D. Xu and X. Zhang, *Mater. Res. Bull.*, 2011, **46**, 1524.
12. J. Zhou, G. L. Zhao, B. Song and G. R. Han, *Crystengcomm*, 2011, **13**, 2294.
13. J. G. Li, T. Ishigaki and X. D. Sun, *J. Phys. Chem. C*, 2007, **111**, 4969.
14. C. C. Wang and J. Y. Ying, *Chem. Mater.*, 1999, **11**, 3113.
15. R. L. Penn and J. F. Banfield, *Geochim. Cosmochim. Acta*, 1999, **63**, 1549; X. F. Yang, H. Konishi, H. F. Xu and M. M. Wu, *Eur. J. Inorg. Chem.*, 2006, 2229.
16. G. W. Lu, C. Li and G. Q. Shi, *Chem. Mater.*, 2007, **19**, 3433.
17. J. Takahashi, H. Itoh, S. Motai and S. Shimada, *J. Mater. Sci.*, 2003, **38**, 1695; N. G. Park, J. van de Lagemaat and A. J. Frank, *J. Phys. Chem. B*, 2000, **104**, 8989.
18. F. Hao, H. Lin, C. Zhou, Y. Z. Liu and J. B. Li, *Phys. Chem. Chem. Phys.*, 2011, **13**, 15918.
19. Q. Wang, J. E. Moser and M. Gratzel, *J. Phys. Chem. B*, 2005, **109**, 14945; G. Zhu, L. K. Pan, J. Yang, X. J. Liu, H. C. Sun and Z. Sun, *J. Mater. Chem.*, 2012, **22**, 24326; Z. He, G. Guai, J. Liu, C. Guo, J. S. Chye Loo, C. M. Li and T. T. Y. Tan, *Nanoscale*, 2011, **3**, 4613; Z. He, H. Phan, J. Liu, T.-Q. Nguyen and T. T. Y. Tan, *Adv. Mater.*, 2013, 10.1002/adma.201303327.
20. L. De Marco, M. Manca, R. Giannuzzi, F. Malara, G. Melcarne, G. Ciccarella, I. Zama, R. Cingolani and G. Gigli, *J. Phys. Chem. C*, 2010, **114**, 4228.
21. Q. F. Zhang and G. Z. Cao, *Nano Today*, 2011, **6**, 91.